Penerbit Akademia Baru

Journal of Advanced Research in Applied Mechanics
ISSN (online): 2289-7895 | Vol. 20, No. 1. Pages 1-11, 2016

Fractal Cracks Propagation in AISI 410 Steel

M. A. Khattak[*,1,a], *M. A. Amil*[2,3,b], *M. N. Tamin*[2,c], *M. Mat Noh*[2,d], *N. Sulaiman*[2,e] *and T. A. Mohamed Nori*[2,4,f]

[1]Department of Nuclear Engineering, Faculty of Chemical and Energy Engineering, Universiti Teknologi Malaysia, 81310 Skudai Johor, Malaysia
[2]Department of Applied Mechanics and Design, Faculty of Mechanical Engineering, Universiti Teknologi Malaysia, (UTM), Johor, Malaysia.
[3]Faculty of Engineering, Universiti Selangor (UNISEL), 45600 Bestari Jaya, Selangor, Malaysia
[4]Forensic Engineering Division, Department of Occupational Safety & Health, 62530, Putrajaya, Malaysia
*,[a]*muhdadil@utm.my*, [b]*azril@unisel.edu.my*, [c]*taminmn@fkm.utm.my*, [d]*mazmir.mn@gmail.com*, [e]*ikinnora@gmail.com*, [f]*tajul_ariffin7@yahoo.com*

Abstract – *In this research work, an experimental investigation was conducted to explore fractal dimension (D) evaluation from crack path data through fractal geometry analysis. Hence, proving the possibility of demonstration of a valid relationship between KIC and the fractal dimension (D) for AISI 410 stainless steel. Compressor blades in power generating industries are commonly made of AISI 410 stainless steel. Evolution in microstructure properties and chemical composition of the material has also been investigated. The structure reveals matrix of equiaxed ferrite grains, with randomly dispersed particles of chromium carbide. Fatigue crack growth test is conducted on compact tension C(T) specimen at constant load ratio of minimum to maximum stress, R = 0.1. All tests are performed at room temperature for baseline fatigue crack growth behavior. Results showed that the fatigue crack growth rate behavior displays a threshold growth stage followed by a power-law growth region until final fracture of the specimen. The threshold ΔKth comes out to be 14.7 MPa√m.*

Keywords: AISI 410 Steel, FCGR, Fractals, Crack Propagation, Fractal Dimension

1.0 INTRODUCTION

Advancements made in the field of materials have contributed in a major way in building gas turbine engines with higher power ratings and efficiency levels [1-2]. Improvements in design of the gas turbine engines over the years have importantly been due to development of materials with enhanced performance levels. Gas turbines have been widely utilized in power generation industry across the globe [3]. Gas turbines in power generating plants are commonly equipped with compressor blades made of martensitic stainless steels [4]. These turbines operate at nominal speed of 7500 rpm (8.5 MW) and temperature ranges up to 500 – 600 °C [5]. The spinning impeller induces centrifugal forces resulting in relatively large stresses in the blades. Such high-frequency small amplitude vibration could contribute to high-cycle fatigue failure of the blades that leads to the initiation of crack-like defects, thus detrimental to effective performance and design life of the compressor blade material [6]. Accurate prediction and improvement of compressor blades material reliability requires the evolution and application

of engineering models [7]. These models are based on an understanding of the failure modes and the statistical distributions of the controlling parameters [8]. This can be achieved through a combination of classical Fracture Mechanics with Fractal analysis.

Fractal geometry developed so far has been successfully used to describe quantitatively complex shapes such as fracture surfaces in metal, ceramics and polymeric materials [9]. This approach represents a novel way to quantitatively characterize the topography of a surface. Fractal parameter provides a measurement for the irregularity of curves described. Fracture surface analysis, by fractal geometry, has been applied to distinguish the geometrical effects of different fracture mechanisms [10-12]. For several metallic materials, a direct correlation between fracture toughness and the fractional part of the fractal dimension has been found [13-15]. Recently, it is found that the fractal analysis of crack profile also proves to be an effective way to characterize the geometrical effects of different fracture mechanisms [16-18].

Nomenclature

a	crack dimension	μ	ruler
a_i	threshold crack dimension	$G(\mu)$	counter
a_f	critical crack dimension	D	fractal dimension
N	number of fatigue cycles	E	Youngs' module
ΔK	stress-intensity factor range	n	Poisson coefficient
ΔK_{th}	threshold stress-intensity factor	ρ	density
K_c	critical stress-intensity factor	σ_s	yield stress
C, n	material constants of Paris–Erdogan's law (see Eq. (1))	σ_r	ultimate tensile stress
		σ_{LA}	fatigue strength (2×10^6 cycles)
Y	parameter of element geometry in Paris–Erdogan's Law (see Eq. (1))	k_t	stress-concentration factor
		ω	loading frequency
σ	stress	R	stress ratio
AE	acoustic emission	M_f	bending moment
η	number of AE counts	dof	degree-of-freedom
B, α	parameters dependent of material		

The present research involved the investigation of fracture processes by analysing the geometrical features of the crack profiles instead of fracture surfaces. The crack paths were analysed to achieve information about the toughening mechanisms involved. Fractal geometric analysis, when applied to a crack profiles, provides a measure of its irregularity which can be correlated to the plane-strain fracture toughness, KIC. The present study is intended to suggest best available practices and procedures for fractal analysis, demonstrate a relationship between KIC and the fractal dimension (D) for AISI 410 stainless steel. In this regard, the contributions of this paper are as follow;

- Measurement of crack surface propagation during fatigue crack growth process.
- Analysis of crack path data using methods of fractal geometry.

2.0 MATERIALS AND EXPERIMENTAL PROCEDURES

The material employed in this study is an AISI 410 martensitic stainless steel which was received in the form of circular plate with radius and thickness of 440 mm and 18 mm, respectively. It was wire-cut using Electrical Discharge Machine (EDM) into dog-bone shaped specimen for tensile testing. Figure 1 illustrates the dimension details of the dog-bone shaped specimen with a gage length of 25 mm.

Penerbit Akademia Baru

Journal of Advanced Research in Applied Mechanics
ISSN (online): 2289-7895 | Vol. 20, No. 1. Pages 1-11, 2016

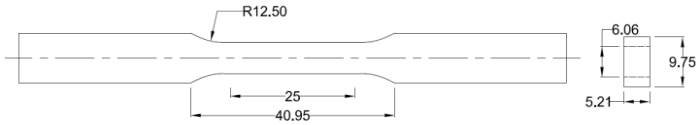

Figure 1: Geometry of dog-bone shaped specimen (dimensions in mm)

For microstructural study, the material was observed at three orthogonal section planes. The microstructural observations were obtained and the images of the microstructure at different magnification were captured using Optical Microscope equipped with image analyser.

The chemical composition of the material was established using Glow Discharge Spectrometry (GDS) machine and is shown in Table 1. The primary alloying elements are chromium (Cr) and carbon (C). AISI 410 martensitic stainless steel have higher amount of carbon and chromium to obtain high strength, high toughness and good corrosion resistance while manganese and nickel contribute to improved toughness of the steel. Generally, the chromium and carbon content for martensitic stainless steel lies between 0.08 – 1.10 % for carbon and 12 – 18 % for chromium [30]. Results obtained from GDS for the selected material revealed that the carbon and chromium content are 0.15 and 14.2 %, respectively.

Table 1: Chemical composition (in weight percent) of AISI 410 stainless steel

Material	C	Mn	P	S	Si	Cr	Ni	Mo	Al	V	Fe
AISI 410	0.2	0.5	0.02	0.002	0.35	14.20	0.39	0.01	0.003	0.03	Bal.

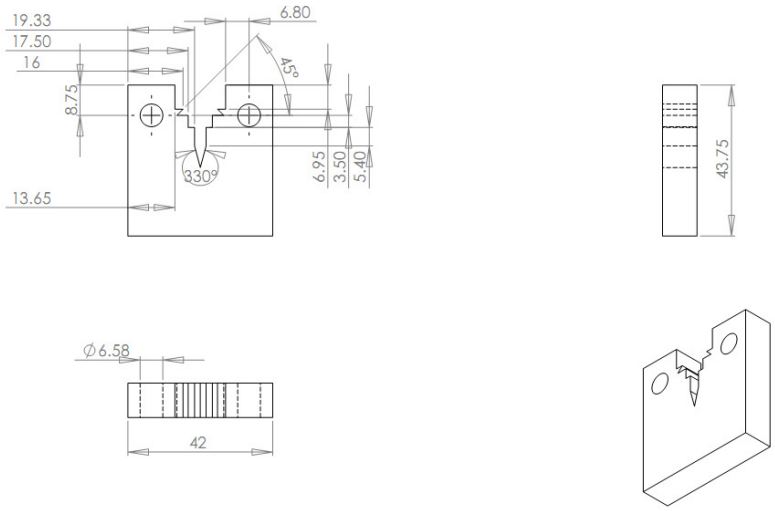

Figure 2: Geometry and dimensions of CT Specimen

Compact tension (CT) specimens were designed according to ASTM E647-13 (Figure 2). In each specimen, a sharp notch was wire cut to facilitate fatigue pre-cracking. The specimen was mirror polished to aid in identifying the fatigue crack tip. Crack lengths were measured using a traveling microscope with 10X optics.

Fatigue pre-cracking procedure is employed to establish and initial crack, a, in the center-cracked specimen. Fatigue crack growth rate tests were also conducted in accordance to ASTM

Journal of Advanced Research in Applied Mechanics
ISSN (online): 2289-7895 | Vol. 20, No. 1. Pages 1-11, 2016

E647-13 procedures. The tests were performed using Instron 8801, ±100 kN servo-hydraulic testing machine under load control mode. Fatigue loading consists of load range ΔP = 2.41 kN, load ratio R = 0.1 and loading frequency of 10 Hz. Finally, measurement of the crack surface propagation was carried out using crack path data through fractal geometry analysis.

3.0 RESULTS AND DISCUSSION

3.1 Microstructure

For microstructural study, the material was observed at three orthogonal section planes. The microstructural observations were obtained and the images of the microstructure at different magnification were captured using Optical Microscope equipped with image analyser. For sample preparation, the specimens were finely grind, polished and etched in the etching solution (5 ml HCL + 2gr Picric acid + 100 ml Ethyl alcohol) for approximately 7 seconds.

Figure 3 shows microstructures of the AISI 410 martensitic stainless steels at the three different orthogonal section planes. The microstructure shows a typical body-cantered tetragonal (bct) structure. The dark area represents martensitic phase while light area shows the ferrite phase. The structure reveals the matrix of equiaxed ferrite grains, with randomly dispersed particles of chromium carbide. Since qualitatively identical microstructure is displayed for each section, the material is expected to behave in isotropic manner.

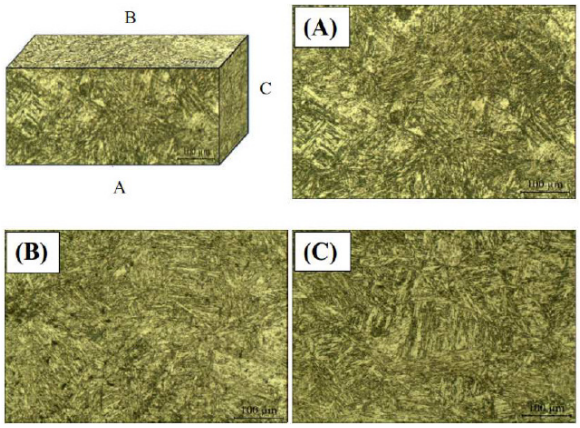

Figure 3: Microstructure observations for section A, B and C

3.2 Tensile Testing

To obtain the mechanical properties of the respective material as shown in Table 2, tensile test was performed on the dog bone shaped specimen.

Table 2: Mechanical properties of AISI 410 steel at room temperature

Material	Tensile Strength (MPa)	Yield Strength (MPa)	Elongation (pct.)	Maximum Load (kN)
AISI 410	656.04	620.17	30	21.27

3.3 Fatigue Crack Growth Behaviour

Penerbit Akademia Baru

Journal of Advanced Research in Applied Mechanics
ISSN (online): 2289-7895 | Vol. 20, No. 1. Pages 1-11, 2016

Fatigue crack growth behaviour of AISI 410 steel examined in this study is compared in Fig. 4 in terms of normalized crack length, a, versus loading cycles, N. For each test, crack grows initially at slow rate but accelerates as the crack length increases after accumulating larger number of cycles. This is consistent with the increase in stress intensity factor ranges as crack lengthens. Final fracture on each curve is represented by the last point during the fatigue crack growth testing.

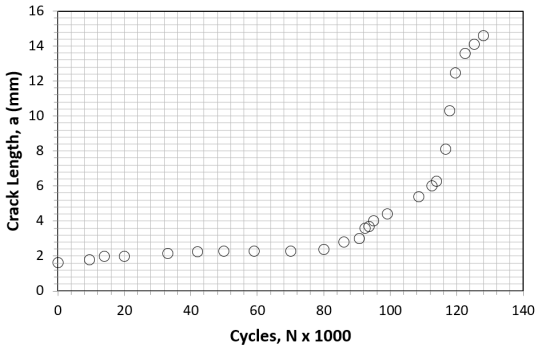

Figure 4: Fatigue crack growth behaviour of AISI 410 steel

It is noted that the material endured the longest life of 128000 cycles and a catastrophic fracture occurred after the final crack length reached larger than 10.5 times their initial length.

Fig. 5 shows the fatigue crack growth rate behavior of AISI 410 steel. The fatigue crack growth rate, da/dN is plotted against the applied stress intensity factor range, ΔK. Fatigue crack growth behavior of AISI 410 steel shows a threshold growth stage followed by a power-law growth behavior until final fracture of the specimens. The threshold, ΔK_{th}, draws a limiting value range for stress intensity, below which the existing crack in the structure will not grow.

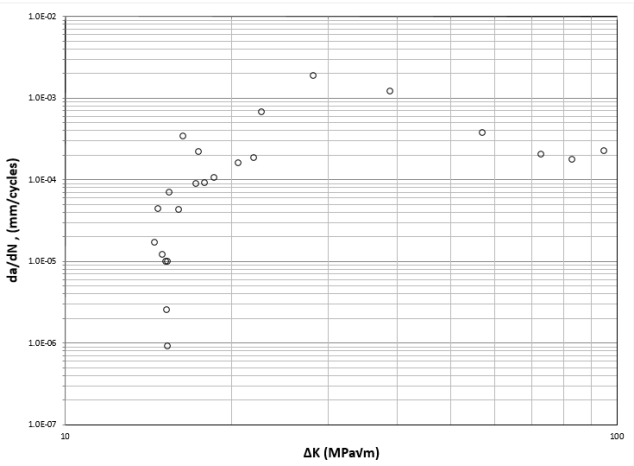

Figure 5: Fatigue crack growth rates of AISI 410 steel

The measured value of threshold ΔK_{th} is 14.7 MPa√m for AISI 410 steel. In the power-law growth region, the crack growth rate is normally represented by Paris equation. In this region, da/dN ranges from 10^{-5} to 10^{-3} mm/cycle while the crack-tip driving force, ΔK varies from 14 to 28 MPa√m. The magnitude of ΔK at the final fracture is about 38.8 MPa√m which approximate the fracture toughness of the AISI 410 steel. The measured value of paris coefficient (n) was 9.74 (Figure 6).

Penerbit Akademia Baru

Journal of Advanced Research in Applied Mechanics
ISSN (online): 2289-7895 | Vol. 20, No. 1. Pages 1-11, 2016

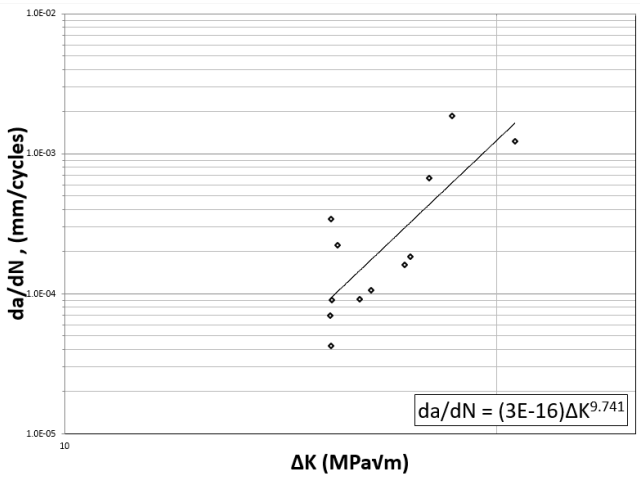

Figure 6: Paris region of fatigue crack growth of AISI 410 steel

3.4 Fractal Analysis

The basic principle to estimate fractal dimension is based on the concept of self-similarity. Consider a non-empty bounded subset F in the Euclidean space $\mathbb{R}^n$, where $n \in \mathbb{N}$. The set F is said to be self-similar when F is the union of N(r) distinct (non-overlapping) copies of itself each of which is similar to F scaled down by a ratio r. The most popular way to calculate the fractal dimension is by box-counting [22]. Let N(r) be the smallest number of sets of diameter r, with $0 < r \ll 1$, which covers F. Then, the lower and upper box dimensions of F are, respectively, defined [23] as follows:

$$\underline{D}_F \triangleq \liminf_{r \to 0^+} \frac{\log_2 N(r)}{-\log_2 r} \quad \text{and}$$

$$\overline{D}_F \triangleq \limsup_{r \to 0^+} \frac{\log_2 N(r)}{-\log_2 r}$$

If the above two limits are equal, then the box dimension DF of F is defined as

$$D_F \triangleq \lim_{r \to 0^+} \frac{\log_2 N(r)}{-\log_2 r}. \qquad (1)$$

3.4.1 Data Acquisition

A Specimen of AISI 410 Martensitic Stainless Steel from fatigue crack growth experiment were observed under Alicona Infinite Focus. The images were captured using digital high resolution camera (20x, 50x, 100x magnification). Alicona Infinite Focus used rather than optical microscope or Scanning Electron Machine (SEM) due to convenience of the image are uniformly scale and stitched together. If using either optical microscope or SEM machine, loads of images need to be stitched together manually as both equipment can't capture the whole solid image of crack. Worry that it will affect the accuracy of total output for the fractal analysis. Figure 7 shows the image sample of crack captured. Total crack length in this sample is a = 4.26mm.

Penerbit Akademia Baru

Journal of Advanced Research in Applied Mechanics
ISSN (online): 2289-7895 | Vol. 20, No. 1. Pages 1-11, 2016

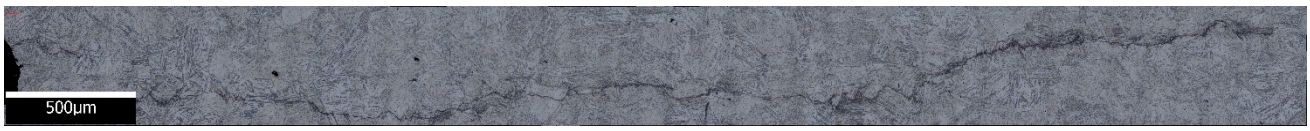

Figure 7: Crack image captured from Alicona Infinite Focus (100X magnification)

3.4.1 Pre-Processing

Raw crack image captured can't be immediately analyzed by fractal analysis. The image has too much noise and need to be cleaned/processed. The crack image has been excerpted from original raw digital image, applying the imaging software (Adobe Photoshop; GIMP etc.). The raw digital image from optical study are converted into a gray level (binary image) with only two color pixel (black and white) as shown in Figure 8

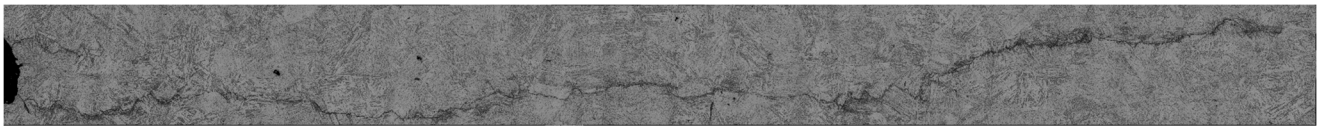

Figure 8. Black and white (Two colour pixel)

Segmentation of image are done manually for more accurate crack edge recognition. The path selection tool is use to manually select the crack boundary. The final crack image that fit for analyzing is shown in Figure 9 below.

3.4.2 Fractal Evaluation

In this study, Minkowski-Bouligand Method (box counting method) is employed to compute the fractal dimensions. The method is done by assigning the smallest number of boxes to cover the entire image surface at each selected scale as required and obtained more accurate estimation of fractal dimension. For the ease of counting, MATLAB algorithm are used in this project to calculates the covered area of crack. Area fall in the box, are counted. This method/steps had been widely used by past researchers such as [19-21].

From MATLAB algorithm, the plot of log N(r) vs log (r) as shown in

Figure 10. The slope of the curve represents the fractal dimensions. For self-similar characteristic, the gradient line should have constant slope, i.e. the dimension in the smallest scale in equal to dimension in larger scale. However, there is some deviation in the slope when the size, r reach 1000.

Penerbit Akademia Baru

Journal of Advanced Research in Applied Mechanics
ISSN (online): 2289-7895 | Vol. 20, No. 1. Pages 1-11, 2016

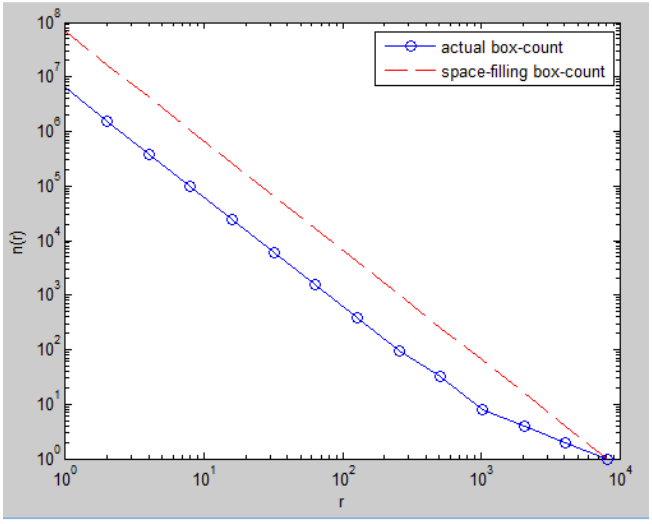

Figure 10: The plot of log N(r) vs log (r)

Theoretically, if we assumed that the crack is fractal, then the fractal dimension of each box scale should have similar value of D. From the plot as per Figure 11, it has shown that the fractal dimension is linear from the range less than 1000 of box size. This should imply that there is an upper boundary of box size to select for fractal to make. From the plot, it is proven that the fractal dimension compute from the MATLAB program fall within the range of 1.15-1.22.

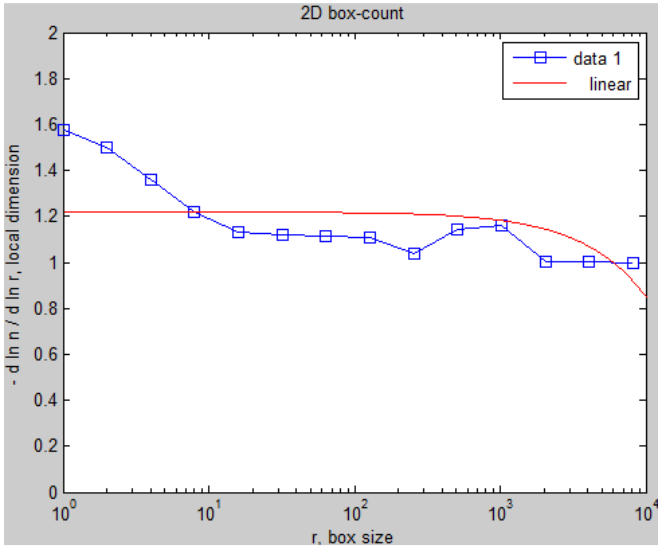

Figure 11: Fractal Dimension value when crack length, a = 4.26 mm

4.0 CONCLUSIONS

Major conclusions from the study are;

- The microstructure of AISI 410 steel shows a typical body-cantered tetragonal (bct) structure. Since qualitatively identical microstructure is displayed for all three sections, the material is expected to behave in isotropic manner.
- The low crack growth rate region is characterized by crack growth bridging process. At higher stress intensity factor range, the crack growth rate, da/dN increases with increasing applied ΔK.
- Fractal Dimension (D) is evaluated from crack path data through fractal geometry analysis. Therefore, it is possible to demonstrate a relationship between K_{IC} and the fractal dimension (D) for AISI 410 stainless steel.

ACKNOWLEDGEMENT

This project is supported by the Ministry of Science, Technology and Innovation (MOSTI), Government of Malaysia through e-Science Fund Project No. 4F561 and Forensic Engineering Division, Department of Occupational Safety & Health, 62530, Putrajaya, Malaysia.

REFERENCES

[1] Oskarsson, H. "Material challenges in industrial gas turbines." Journal of Iron and Steel Research, International 14, no. 5 (2007): 11-14.

[2] Wright, Ian G., and T. B. Gibbons. "Recent developments in gas turbine materials and technology and their implications for syngas firing." International Journal of Hydrogen Energy 32, no. 16 (2007): 3610-3621.

[3] Konter, M., and M. Thumann. "Materials and manufacturing of advanced industrial gas turbine components." Journal of Materials Processing Technology 117, no. 3 (2001): 386-390.

[4] Klotz, Ulrich E., Christian Solenthaler, and Peter J. Uggowitzer. "Martensitic–austenitic 9–12% Cr steels—Alloy design, microstructural stability and mechanical properties." Materials Science and Engineering: A 476, no. 1 (2008): 186-194.

[5] Siemens, “A Full Range of World-class Industrial Steam Turbines,” *2009*.

[6] Witek, Lucjan. "Crack propagation analysis of mechanically damaged compressor blades subjected to high cycle fatigue." Engineering Failure Analysis 18, no. 4 (2011): 1223-1232.

[7] Troshchenko, V. T., and A. V. Prokopenko. "Fatigue strength of gas turbine compressor blades." Engineering failure analysis 7, no. 3 (2000): 209-220.

[8] Kermanpur, A., H. Sepehri Amin, S. Ziaei-Rad, N. Nourbakhshnia, and M.

Journal of Advanced Research in Applied Mechanics
ISSN (online): 2289-7895 | Vol. 20, No. 1. Pages 1-11, 2016

Mosaddeghfar. "Failure analysis of Ti6Al4V gas turbine compressor blades." Engineering Failure Analysis 15, no. 8 (2008): 1052-1064.

[9] Mandelbrot, Benoit B., Dann E. Passoja, and Alvin J. Paullay. "Fractal character of fracture surfaces of metals." (1984): 721-722.

[10] Mecholsky, John J. "Estimating theoretical strength of brittle materials using fractal geometry." Materials Letters 60, no. 20 (2006): 2485-2488.

[11] Carpinteri, Andrea, and Andrea Spagnoli. "A fractal analysis of size effect on fatigue crack growth." International journal of fatigue 26, no. 2 (2004): 125-133.

[12] Borodich, Feodor M. "Fractals and fractal scaling in fracture mechanics." International Journal of Fracture 95, no. 1-4 (1999): 239-259.

[13] Sakai, Takashi, and A. Ueno. "Fractal and fracture mechanics analyses on fatigue fracture surfaces of metallic materials." In ICF10, Honolulu (USA) 2001. 2013.

[14] Carney, Luis R., and John J. Mecholsky Jr. "Relationship between fracture toughness and fracture surface fractal dimension in AISI 4340 steel." (2013).

[15] Bouchaud, Elisabeth, G. Lapasset, and J. Planes. "Fractal dimension of fractured surfaces: a universal value?." EPL (Europhysics Letters) 13, no. 1 (1990): 73.

[16] Tarafder, Mita, S. K. Das, I. Chattoraj, M. Nasipuri, and S. Tarafder. "Fractal-based quantification of crack paths for determination of effective microstructural length scales and fracture toughness." Scripta Materialia 62, no. 2 (2010): 109-112.

[17] Horvath, V. K., and H. J. Herrmann. "The fractal dimension of stress corrosion cracks." Chaos, Solitons & Fractals 1, no. 5 (1991): 395-400.

[18] Jing, L. I., Yan-Sheng Yin, and Ying-Cai Liu. "Fractal analysis of crack paths in Al 2 O 3-TiC-4% Co composites." Transactions of Nonferrous Metals Society of China 16, no. 4 (2006): 795-799.

[19] Carpinteri, Andrea, and Andrea Spagnoli. "A fractal analysis of size effect on fatigue crack growth." International journal of fatigue 26, no. 2 (2004): 125-133.

[20] Wang, Lu, Zheng Wang, Weiyun Xie, and Xigeng Song. "Fractal study on collective evolution of short fatigue cracks under complex stress conditions." International Journal of Fatigue 45 (2012): 1-7.

[21] Jha, Devesh K., Dheeraj S. Singh, S. Gupta, and A. Ray. "Fractal analysis of crack initiation in polycrystalline alloys using surface interferometry." EPL (Europhysics Letters) 98, no. 4 (2012): 44006.

[22] Sarkar, Nirupam, and B. B. Chaudhuri. "An efficient differential box-counting approach to compute fractal dimension of image." Systems, Man and Cybernetics,

Journal of Advanced Research in Applied Mechanics
ISSN (online): 2289-7895 | Vol. 20, No. 1. Pages 1-11, 2016

IEEE Transactions on 24, no. 1 (1994): 115-120.

[23] Falconer, Kenneth. Fractal geometry: mathematical foundations and applications. John Wiley & Sons, 2004.